Tuijin Jishu/Journal of Propulsion Technology
ISSN: 1001-4055
Vol. 47 No. 04 (2026)

Green Synthesis, Molecular Docking and In Silico ADMET Profiling of Novel Phenacetamido-Pyrazoline Derivatives as Potential Cathepsin K-Targeted Antiresorptive and Cyclooxegenase agent

Jayapriya murugan[1], Arumugam Kannan[1] and Rajalakshmi Ramarajan[1]*
[1, 1*] Department of Chemistry, Annamalai University, Annamalainagar 608002, Tamil Nadu, India.

Abstract:- A series of phenacetamido-pyrazoline derivatives (7a–g) was synthesized using a recyclable ionic liquid catalyst under mild and environmentally friendly conditions, achieving yields of up to 90%. The structures of the synthesized compounds were confirmed by FT-IR, ^{1}H NMR and ^{13}C NMR spectroscopy. Molecular docking studies were conducted against cathepsin K and cyclooxygenase-2 (COX-2), using balicatib, diclofenac and celecoxib as reference drugs for the respective targets. Compound 7f exhibited a docking score of −7.32 kcal/mol against cathepsin K PDB ID: 1ATKand −9.93 kcal/mol against the protein identified by PDB ID 1CVU. In silico ADMET and ProTox-III analyses indicated potentially favourable pharmacokinetic properties and toxicity profiles. Density functional theory (DFT) and frontier molecular orbital (FMO) analyses further characterized the electronic properties of the derivatives. Overall, these findings highlight compound 7f as a promising candidate for further investigation of its potential biological and anti-inflammatory activities.

Keywords: Anti -diabetic, Anti-fungal, Swiss ADMET, chalcone, phenacetamido-pyrazoline, protox III, cathepsin inhibitors, Anti-resportive

1. Introduction

The surging global demand for advanced functional materials and high-value bioactive entities has driven a heavy reliance on traditional volatile organic solvents. Conventional reaction media and corrosive catalysts pose severe environmental and health hazards due to their high volatility, toxicity and unsustainable lifecycles. To address these drawbacks, contemporary organic synthesis has shifted dramatically toward Green Chemistry principles. Within this framework, ionic liquids (ILs) and supported ionic liquids (SILs) have gained exceptional attention as viable, eco-friendly alternatives. Characterized by negligible vapor pressure, broad liquid-phase temperatures and highly tunable solvation properties, IL networks act simultaneously as green reaction media and homogeneous catalysts. They stabilize charged transition states, facilitate proton-transfer steps via hydrogen bonding and accelerate cyclization processes. Furthermore, immobilizing ILs on solid matrices enables seamless catalyst recovery and multi-cycle reuse, ensuring simplified product isolation and minimized waste [1-5]. Diabetes mellitus and fungal infections are rising global health threats worsened by drug resistance [6-8]. Diabetes causes chronic hyperglycemia and severe systemic complications, which are managed by inhibiting α-amylase and α-glucosidase to limit glucose absorption, or targeting PPAR-γ to improve insulin sensitivity [9-10]. Immunocompromised individuals face severe risks from *Candida albicans* and *Aspergillus niger* [11-13]. To combat resistance, current drug development focuses heavily on inhibiting lanosterol α -demethylase (CYP51), an essential enzyme in fungal cell membrane ergosterol biosynthesis, to trigger membrane dysfunction and cell death [14-16]. Phenacetamido-pyrazoline derivatives represent an important class of heterocyclic compounds known for their diverse range of pharmacological activities notably anti-inflammatory,

antimicrobial, antitubercular, antiviral, anticancer, antioxidant, antidiabetic and various enzyme inhibitor effects [17-18]. Several phenacetamido-pyrazoline based agents have already achieved clinical success, underlining their significance in drug development. The interplay between structural variation and biological function underscores the need for sustainable methodologies that can expediently access novel phenacetamido-pyrazoline derivatives with enhanced activity and drug-like properties [19-21]. Concurrently, the design of novel small-molecule heterocycles occupies a central position in medicinal chemistry to combat escalating global health crises. Among nitrogen-containing five-membered frameworks, 2-pyrazolines have emerged as privileged scaffolds. The synthetic versatility of the pyrazoline nucleus allows for strategic functionalization, making it an ideal core for molecular hybridization [22-25]. Integrating a structurally rigid phenacetamido fragment onto the pyrazoline core offers a synergistic approach to generating hybrid molecules with optimized pharmacokinetic profiles, altered lipophilicity and enhanced hydrogen-bonding capacity. Similarly, integrating pyrazoline and phenacetamido- pyrazoline nuclei provides access to highly pharmacologically active structural architectures. Traditional synthetic pathways toward these diverse systems frequently suffer from prolonged thermal activation, hazardous reagents and low atom economy, making the development of mild, solvent-minimized protocols an urgent frontier [26]. Bone remodeling maintains skeletal integrity through a fine balance between osteoclastic resorption and osteoblastic formation. An imbalance where resorption exceeds formation leads to metabolic bone disorders, primarily osteoporosis, characterized by reduced bone mass, microarchitectural deterioration, and heightened fracture risk. Current antiresorptive therapies, including bisphosphonates and hormone replacement, are constrained by severe long-term side effects such as osteonecrosis of the jaw and atypical fractures. Consequently, there is an urgent need for novel, safer small-molecule therapeutics.

Heterocyclic cores, particularly pyrazoline derivatives, represent a privileged class of compounds displaying diverse pharmacological profiles, including cyclooxygenase (COX) inhibitory, anti-inflammatory, antioxidant, antidiabetic and antifungal activities. Concurrently, incorporating a phenylacetamido moiety into heterocyclic frameworks enhances structural stability, pharmacokinetic properties and target binding affinity. Given that COX-mediated inflammatory signaling, metabolic dysfunction and oxidative stress are intrinsically linked to accelerated osteoclastogenesis and systemic bone loss, targeting these converging pathways with multifunctional scaffolds presents a compelling therapeutic approach.Motivated by these considerations, this study describes the design, synthesis and structure–activity relationship (SAR) evaluation of novel phenylacetamido pyrazoline derivatives. We investigate the ability of these hybrid molecules to inhibit COX-mediated inflammatory signaling and RANKL-induced osteoclast differentiation, offering valuable insights into the development of next-generation agents for managing osteoporosis and related metabolic bone disorders.

This study focuses on the design, synthesis and structure–activity relationship (SAR) evaluation of novel phenacetamido pyrazoline derivatives for inhibiting osteoclast differentiation and bone resorption, alongside assessing their broader biological potential. Spurred by these dual objectives, this work describes an efficient, green protocol for the synthesis of a novel series of phenacetamido-pyrazoline- derivatives utilizing a highly recyclable ionic liquid-assisted strategy. The newly synthesized hybrids were structurally characterized using Fourier-transform infrared (FT-IR), ^{1}HNMR and ^{13}C NMR spectroscopic techniques.

2. General

All chemicals and solvents were purchased from Sigma-Aldrich, Avra and TCI Chemicals were used as received without further purification. Melting points were determined using open-capillary tubes. The purity of the compounds and the progress of the reactions were monitored by thin-layer chromatography (TLC) on silica gel plates under UV light. The mobile phase consisted of a petroleum ether and ethyl acetate solvent system in a 1:3 ratio. Infrared (IR) spectra were recorded in the range of 4000–600 cm^{-1} using an Agilent Resolution spectrometer. ^{1}H and ^{13}C NMR spectra were recorded on a Bruker 400 MHz NMR spectrometer at room temperature using $CDCl_3$ or DMSO-d_6 as solvents. Tetramethylsilane (TMS) was used as the internal standard and chemical shifts were reported in parts per million (ppm).

3. Result and discussion

3.1 Chemistry

The strategy for the synthesis of the novel phenacetamido-pyrazoline derivatives involves three steps, beginning with the formation of chalcones, followed by their cyclization with 4-aminobenzohydrazide and acetylation with phenacyl chloride. This approach was chosen to capitalize on the known bioactivity of 4-aminobenzohydrazide and to construct a novel pyrazoline-based heterocyclic scaffold.

Step 1: Synthesis of (E)-1-(5-bromothiophen-2-yl)-3-(4-substituted phenyl)prop-2-en-1-one Derivatives

(E)-1-(5-bromothiophen-2-yl)-3-(4-substitutedphenyl)prop-2-en-1-onederivatives were synthesized via the Claisen–Schmidt condensation under basic conditions, in which 1-(5-bromothiophen-2-yl) ethanone is allowed with various substituted benzaldehydes in ethanol using sodium hydroxide (NaOH) as the base. Sodium hydroxide generates an enolate ion from the ketone, which attacks the carbonyl carbon of the aldehyde to form a β-hydroxy ketone intermediate. This intermediate subsequently undergoes dehydration to produce the corresponding α, β-unsaturated ketone ((E)-1-(5-bromothiophen-2-yl)-3-(4-substituted phenyl)prop-2-en-1-one). The conjugated system involving the thiophene ring, carbonyl group and aromatic ring contributes to the stability of the resulting chalcones. In general, the reaction is favored by electron-withdrawing substituents on the benzaldehydes, whereas electron-donating substituents decrease their reactivity. The formation of the chalcone derivatives are confirmed by IR spectroscopy, which exhibits the characteristic absorption band of α, β-unsaturated carbonyl group. The synthesized compounds are obtained in good yields (70–89%) and were characterized by melting point determination and spectroscopic analysis.

Step 2: Cyclization of Pyrazoline Derivatives

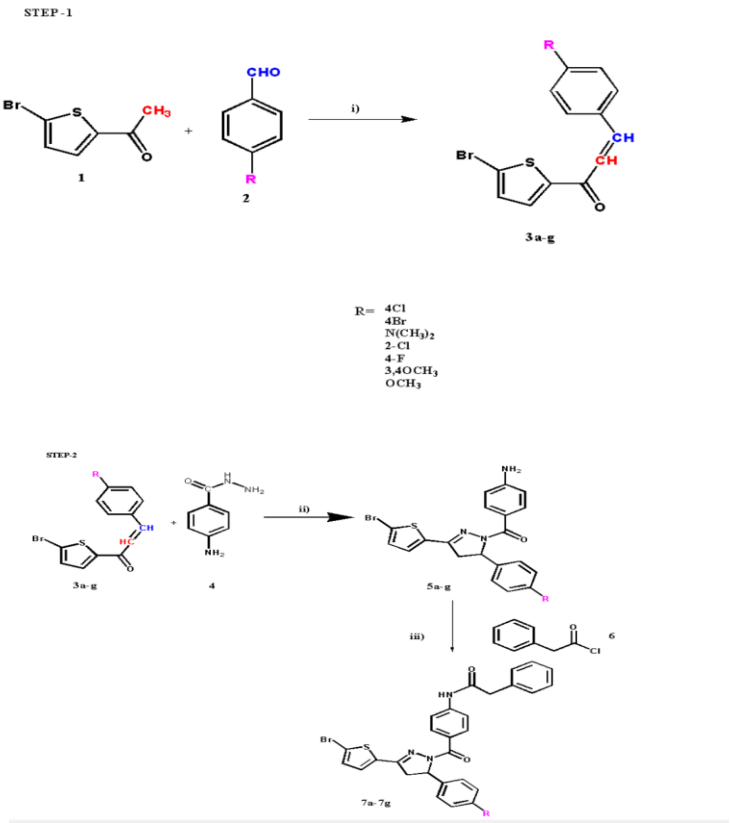
The pyrazoline derivatives (5a–g) were synthesized by the cyclization of (E)-1-(5-bromothiophen-2-yl)-3-(4-substitutedphenyl)prop-2-en-1-one intermediates (3a–g) with 4-aminobenzohydrazide in methanolic potassium hydroxide under reflux conditions. The reaction begins with a Michael addition, in which the nucleophilic nitrogen atom of the hydrazide attacks the electrophilic β-carbon of the α,β-unsaturated chalcone system. The resulting intermediate then undergoes intramolecular cyclization through the attack of the adjacent nitrogen atom on the carbonyl carbon, leading to the formation of the five-membered pyrazoline ring. Subsequent proton transfer and tautomerization complete the formation of the heterocyclic framework, linking the thiophene and substituted phenyl moieties. Furthermore, the electronic nature of the substituents on the aromatic ring influences the reaction rate by effects the electrophilicity of the alternative conjugated double bond, thereby accelerating the cyclization process.

Step 3: N-Acetylation of Pyrazoline Derivatives

The pyrazoline intermediates (5a–g) were subjected to N-acylation with 3-phenylpropanoyl chloride in dichloromethane using 1-allyl-3-methylimidazolium bromide [AMIM]Br] as catalyst. The free para-amino group on the benzamide ring acts as a nucleophile and attacks the carbonyl carbon of the acid chloride, forming a tetrahedral intermediate. There by facilitates reaction by shifting the equilibrium to the highest. Subsequent elimination of chloride ion and deprotonation followed the corresponding amide derivatives (7a–g). The ionic liquid enhances reaction efficiency by providing a highly polar medium that favours the overall reaction N-Acylation under under mild reaction conditions.

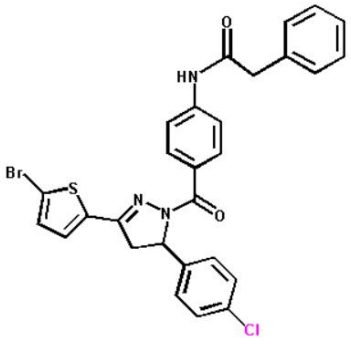
Reusability study of the [AMIM][Br] catalyst

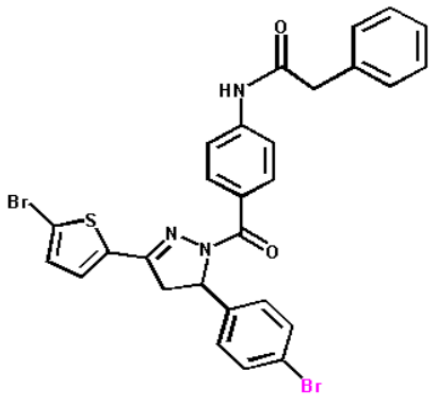
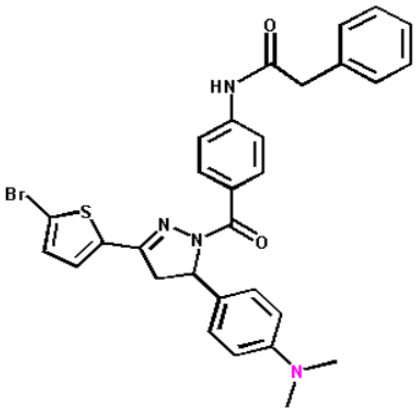
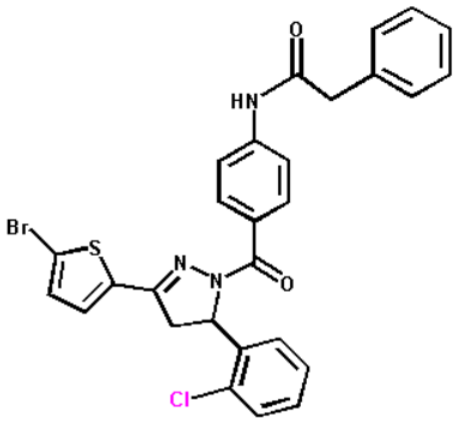
The recyclability of the [AMIM][Br] catalyst were assessed by carrying out a series of model reactions for the synthesis of phenacetamido-pyrazoline derivatives. Upon completion of each reaction, the catalyst is recovered by simple separation and washed to remove any residual impurities, and dried at 70°C for 1 h before being reused. The recovered catalyst maintained its effectiveness over successive reaction cycles, demonstrating its potential for repeated use.

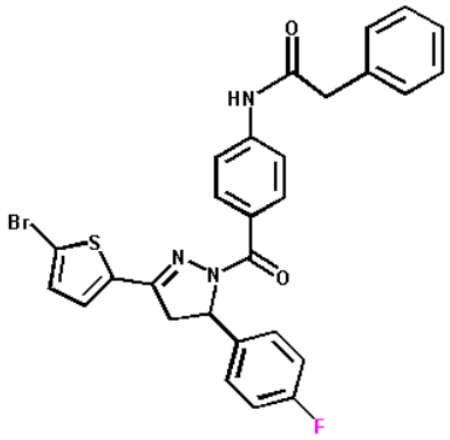
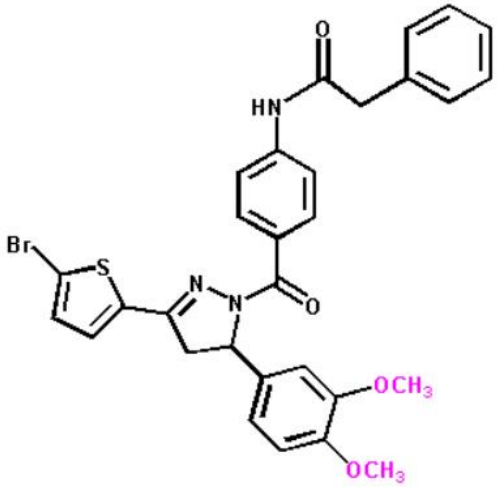
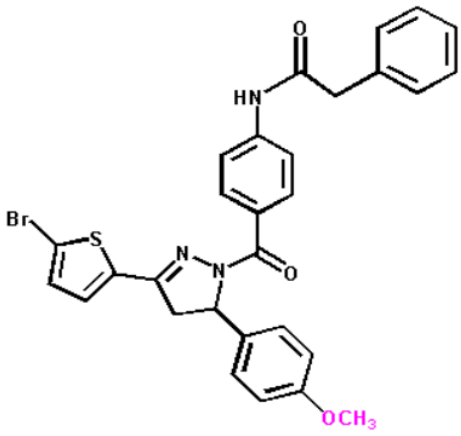


Scheme 1. Synthetic method of phenacetamido-pyrazoline derivatives; i) EtOH, NaOH, stirring 4-7 hrs; ii) R-CONHNH$_2$,KOH, CH_3OH Reflux iii) Phenacetyl chloride, [AMIM]Br,DCM, stirring 2- 4 hrs

Table 1 Structure, yields and M.P of the synthesized compounds (7a-g)

Structure	Yield	M.P
	80%	180 ºC

	69%	150ºC
	78%	180ºC
	72%	175ºC

	76%	165ºC
	74%	190ºC
	78%	185ºC

3.2 Spectral Analysis

All the newly synthesized compounds were characterized by FT-IR, ^{1}H NMR and ^{13}C NMR spectroscopic techniques. The spectral data of all synthesized compounds are found to be consistent with their proposed structures. The FT-IR spectra of the synthesized derivatives show characteristic absorption bands corresponding to N–H stretching vibrations in the range of 3220–3287 cm^{-1}, confirming the presence of the amide NH group.

The carbonyl stretching vibrations appeared in the range of 1640–1670 cm^{-1}, indicating the presence of amide and pyrazoline carbonyl groups. The absorption bands of C=N (pyrazoline ring) stretching vibration are observed at the range of 1580–1602 cm^{-1}, while the bands appearing at 1490–1535 cm^{-1} corresponded to aromatic C=C stretching vibrations. These characteristic absorptions confirmed the formation of the pyrazoline ring and the presence of the expected functional groups in all synthesized compounds.

The ^{1}H NMR spectra of all derivatives recorded in DMSO-d_6 exhibited a characteristic singlet in the range of δ 9.73–10.55 ppm, attributed to the amide NH proton. The aromatic protons of phenyl and thiophene ring appears as multiplet within the range of δ 6.53–7.95 ppm. The characteristic pyrazoline peaks corresponding to CH_2 and CH protons ,C5 and C4 are observed in the range 5.54-5.75 ppm and2.92-3.96 ppm .while the methylene protons of the phenylacetamide moiety (–$COCH_2Ph$) are observed as a singlet in the range of δ 3.60–3.68 ppm. The derivatives containing methoxy substituents show additional singlet signals corresponding to –OCH_3 groups at δ 3.84–3.98 ppm, whereas the dimethylamino-substituted derivative displays a characteristic signal for the $N(CH_3)_2$ group at δ 3.08 ppm. The observed proton resonance confirms the successful incorporation of aromatic substituents on the pyrazoline framework.

The ^{13}C NMR spectra further supports the proposed structure of the synthesized compounds. The carbonyl carbons of the amide and pyrazoline carbonyl groups appear in the range of δ 164.2–173.3 ppm. The characteristic resonance of the pyrazoline C=N carbon is observed in the region of δ 149.8–166.3 ppm. The aromatic and thiophene carbons show signals in the range of δ 111.0–144.2 ppm, while the brominated thiophene carbon (C–Br) appear around δ 112.75 ppm. The pyrazoline C-4 and C-5 carbons resonate in the range of δ 45.3–59.4 ppm, confirming the formation of the dihydropyrazole ring. The methoxy carbon atoms appear at δ 52.5–55.6 ppm, and the phenylacetamide methylene carbon is observed around δ 41–43 ppm. Comparison of the spectral data among the synthesized derivatives reveal that the variation of substituents on the aryl ring influences the chemical shifts and physical properties of the compounds, while the characteristic signals of the pyrazoline nucleus remains almost unchanged. Electron-withdrawing substituents such as chloro, bromo and fluoro groups exhibit slight variations in the aromatic proton and carbon resonances, whereas electron-donating groups such as methoxy and dimethylamino substituent produces additional signals corresponding to their respective functional groups. The presence of all the characteristic IR absorptions, together with the expected ^{1}H and ^{13}C NMR resonances, confirms the successful synthesis of the target pyrazoline derivatives.

3.3 Molecular Docking Studies

Molecular docking studies were performed to investigate the binding interactions and predict the binding affinity of the synthesized compounds against the selected protein targets using AutoDock 4.2. The three-dimensional structures of the target proteins, COX-2 (PDB ID: 1CVU) and 1ATK, were selected for the docking analysis. Protein preparation and visualization of ligand–protein interactions were carried out using BIOVIA Discovery Studio. The docking analysis was used to predict the binding orientation of the synthesized compounds within the respective protein binding sites and to evaluate their potential interactions with key amino acid residues.The predicted binding energies were used to compare the relative binding affinities of the synthesized compounds, with more negative docking scores generally indicating more favorable predicted binding. The ligand–protein interaction profiles were further analyzed to identify non-covalent interactions, including hydrogen bonding, hydrophobic interactions, π–π interactions, π–alkyl interactions and other relevant contacts. These interactions provide insights into the possible binding modes and structural complementarity of the compounds within the target proteins. The docking results were subsequently compared with those of the selected reference drugs, where applicable, to identify promising candidates for further biological evaluation.

Molecular docking against 1ATK

The docking score of −7.32 kcal/mol obtained for compound 7f indicates a favorable predicted binding affinity compared with the other compounds evaluated in this study. The interactions involving Trp A:184, Trp A:188, Gln A:21, and Asn A:47 may contribute to the recognition and accommodation of the ligand within the binding

site. The two-dimensional interaction diagram provides detailed information regarding the types of interactions formed, while the three-dimensional representation illustrates the binding orientation and spatial relationship between the ligand and the surrounding amino acid residues. These findings emphasize the importance of the structural features of compound 7f in its predicted binding behavior. Based on the overall docking results, compound 7f was selected as a potential lead molecule for further investigation of its antiresorptive activity. Nevertheless, molecular docking predictions alone are insufficient to establish the inhibitory activity or therapeutic efficacy of a compound. Therefore, further validation through molecular dynamics simulations, binding free-energy analysis, and appropriate in vitro assays is necessary to confirm the stability of the protein–ligand complex and determine the biological relevance of the observed interactions.(Table 2).

Table 2 Molecular docking, binding energy and amino acid residues.

COMPOUNDS	BINDING ENERGY	AMINO ACID RESIDUES
7a	-7.2	PHE A:144, TYR A: 145 ,LYS A :147,ALA A: 197,LYS A : 200
7b	-5.91	LYS A :77, TYR A:74 ,LYS A :66,MET A :97
7c	-6.44	VAL:149, LYS A :176,200,ASN A: 199,ALA A: 197
7d	-6.59	TRP A:188,TRP A:184,ASN A :18,ARG 111
7e	-7.1	ALA A : 197,LYS A :200,ARG A:198,ASN A: 199, ASN A:175,TYR A :151,145,150
7f	**-7.32**	VAL A: 149,LYS A : 176,200,ASN A : 199,ALA A :197
7g	-5.93	GLN A:21,143,TRP A :184
Standard (Balicatib)	-4.78	ASN A:18,TRP A: 184,GLY A: 20,MET A: 64

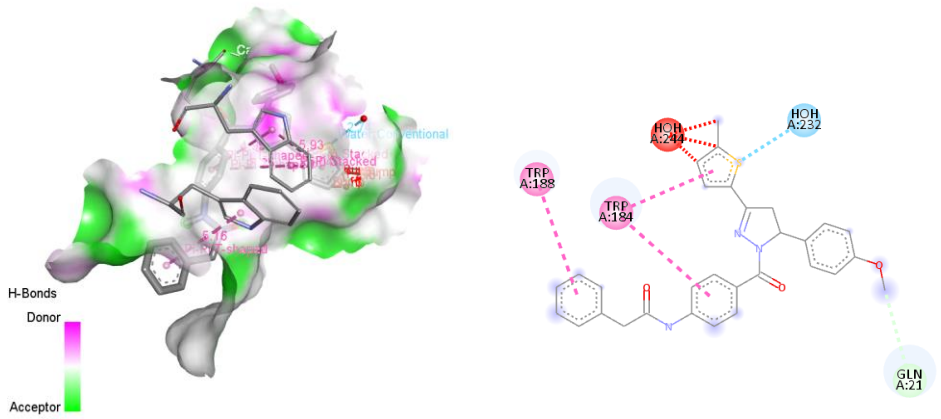


Fig 1: 3D and 2D image of the compound 7f

Molecular docking against 1CVU

Molecular docking studies were performed to investigate the potential anti-inflammatory activity of the synthesized compounds (7a–7g) against cyclooxygenase-2 (COX-2; PDB ID: 1CVU) using AutoDock 4.2. Diclofenac and celecoxib were used as reference drugs for the docking analysis. Among the synthesized compounds, compound 7f exhibited the most favorable predicted docking score of −8.60 kcal/mol, suggesting a

potentially favorable interaction with the COX-2 binding site. The docking results provide preliminary insights into the binding behavior of the synthesized compounds within the target protein.The ligand–protein interaction analysis was performed using BIOVIA Discovery Studio to visualize the binding poses and identify the amino acid residues involved in ligand recognition. Compound 7a showed interactions with Arg120, Tyr355, Ser530, Arg513, Val523 and Phe518, which are associated with the ligand-binding channel and surrounding regions of COX-2. These interactions may contribute to ligand accommodation and stabilization within the binding pocket. The binding orientations and specific interactions of the remaining compounds require evaluation using their respective two-dimensional and three-dimensional interaction diagrams.The reference drugs diclofenac and celecoxib were included to assess their predicted binding modes within the COX-2 binding site. Their docking scores and interaction profiles should be reported according to the verified AutoDock output. Overall, the molecular docking study identifies compound 7f as a promising candidate for further investigation of its potential anti-inflammatory activity. Additional validation through protein–ligand interaction analysis, molecular dynamics simulations and appropriate in vitro biological assays is necessary to establish the stability of the predicted complex and evaluate its biological relevance.(Table 3).

Table 3 Molecular docking, binding energy and amino acid residues.

COMPOUND	BINDING ENERGY	AMINO ACID RESIDUES
7a	-8.68	LEU 224,2145,145,SER 2143,PHE2142,TRP 2139
7b	-9.74	PRO 2153,LEU 2152,PRO 2154,LYS 2459,ASP 2157,ALA 2256,TYR 2136,GLN 327
7c	-7.7	SER 471,LEU 2080,20832,TYR 2115,LYS 2083
7d	-8.24	TYR 2122,LYS 2488,SER 2471,LEU 2472,2080LYS 2083,
7e	-9.35	PRO 2153,2154,LEU 2152,LYS 2459,TYRN2136,ALA 2156,ASP 2157,GLN 327
7f	**-9.93**	ILE 78,TYR 122,115,LEU 75,82,LYS 83,79,VAL 89,PRO 86
7g	-8.34	ARG 44,PRO 86,VAL 89,LYS 83,TYR 122,79
Diclofenac	-6.16	GLNA:374, ARGA:376, ASNA:375, HOH A:3679, HOH B:3528, HOH A:3009, A:3464, A:3132, A:3192, PROA:538, LEUA:145
Celecoxib	-8.14	GluA:46, LysA:137, HOH B:3398, B:3327, B:3455, A:3107, A:3756, A:3412, ProA:153, CysA:41,47,36

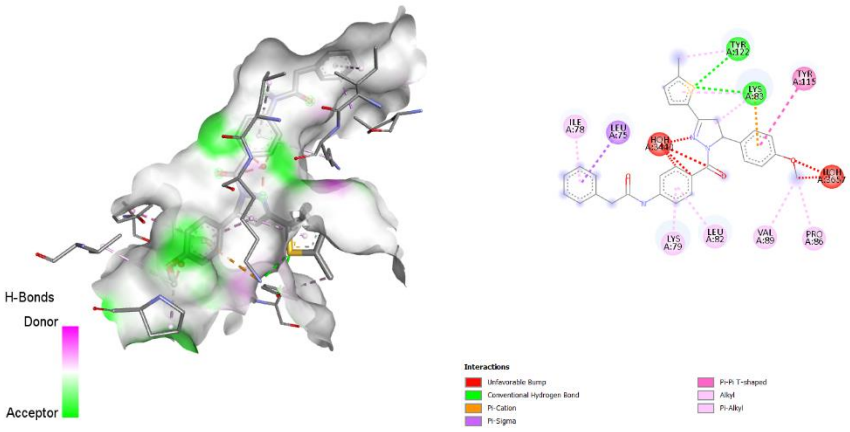


Fig 2: 3D and 2D image of the compound 7f

3.4 Anti-diabetic activity

The *in vitro* antidiabetic efficacy of the synthesized derivatives were evaluated by assessing their inhibitory potential against alpha-amylase, a crucial carbohydrate-hydrolyzing enzyme. The screening was carried out across a concentration range spanning from 25 to 500 µg/mL. All compounds the tested demonstrated a clear, concentration-dependent inhibitory profile against the enzyme. The quantitative percentage of inhibition and the corresponding half-maximal inhibitory concentration IC_{50} values for both the synthesized derivatives and the standard drug (STD) are systematically documented in (Table 4).

Table 4 In Vitro Amylase Inhibitory of the tested compounds

Compound ID	25 µg/mL (%)	50 µg/mL (%)	100 µg/mL (%)	250 µg/mL (%)	500 µg/mL (%)	IC50 (µg/mL)
7a	31.24 ± 1.12	48.91 ± 1.34	62.35 ± 1.05	78.12 ± 0.98	89.47 ± 0.76	51.46 ± 1.24
7b	28.67 ± 0.95	44.32 ± 1.21	59.18 ± 1.42	74.56 ± 1.15	86.23 ± 0.89	59.57 ± 1.53
7c	35.46 ± 1.32	53.45 ± 1.08	67.77 ± 0.94	82.45 ± 1.23	92.31 ± 0.65	25.60 ± 0.88
7d	31.24 ± 1.04	48.91 ± 1.41	62.35 ± 1.18	78.12 ± 1.02	89.47 ± 0.81	51.46 ± 1.19
7e	33.54 ± 1.18	50.18 ± 0.97	64.72 ± 1.35	79.85 ± 1.11	90.36 ± 0.72	49.72 ± 1.05
7f	38.12 ± 1.45	56.78 ± 1.26	71.46 ± 1.02	85.90 ± 0.87	94.82 ± 0.54	40.94 ± 0.92
7g	34.89 ± 1.22	51.42 ± 1.15	66.11 ± 1.29	81.23 ± 0.94	91.05 ± 0.69	47.85 ± 1.12
STD	33.46 ± 0.88	51.33 ± 1.02	65.65 ± 0.91	80.10 ± 0.76	90.11 ± 0.48	46.18 ± 0.75

A comparative analysis of the experimental bioassay data reveals that the specific structural modifications on the parent framework profoundly influences α-amylase inhibition. As shown in (Table 4), compound 7c emerged as the most potent derivative in the entire series, displaying an exceptional IC50 value of 25.60µg/mL, which significantly surpasses the inhibitory efficacy of the standard reference drug IC50 = 46.18µg/mL 7c demonstrated enzyme inhibition of 92.31% at the highest concentration of 500µg/mL. The derivative 7f also showed increased potency compared to the standard with IC value of 40.94µg/mL in (Table 1) and achieved maximum inhibition of 94.82% at 500µg/mL. On the other hand, the methoxy-substituted derivative 7g (IC = 47.85 µg/mL) and the fluorinated analogue 7e (IC = 49.72 µg/mL) showed promising profiles that are still highly comparable to the commercial standard Fig 3.

In contrast, halogenation of the structure produced varied outcomes. As shown in Table 3, both the mono-chlorinated (7a) and di-chlorinated (7d) analogues demonstrated similar moderate .enzyme-inhibitory activity, with each exhibiting an IC value of 51.46 µg/mL. Meanwhile, the brominated analogue 7b was identified as the least active candidate among all screened compounds, exhibiting the highest IC50 the value of 59.57 µg/mL. Taken together, these structure–activity relationship (SAR) insights strongly suggest that the unique electronic distribution and steric features incorporated into the 7c and 7f structural configurations contribute to enhanced binding affinity within the enzyme's active site, making them promising scaffolds for the future development of advanced antidiabetic therapeutics.

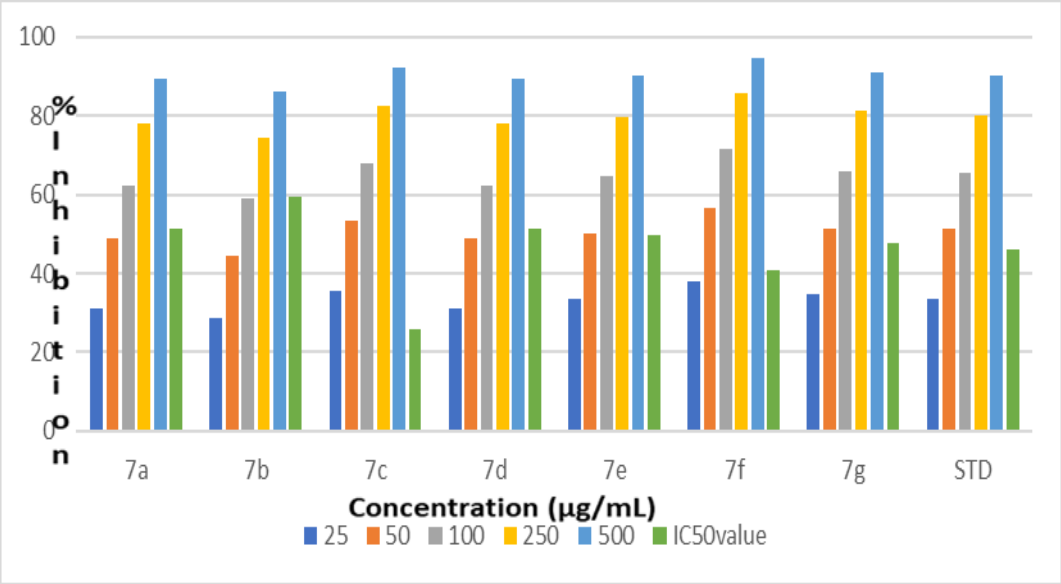


Fig 3. Graphical representation of % inhibition and concentration of the compounds (7a-g)

3.5 Antifungal Activity

In vitro Antifungal activity of the synthesized compounds (7a–g) against *Candida albicans* and *Aspergillus niger*. The results revealed promising antifungal potential, with a clear inverse relationship observed between the zones of inhibition and the minimum inhibitory concentration (MIC) values, where compounds exhibiting larger inhibition zones generally showed lower MIC values. Dimethyl sulfoxide (DMSO), used as the negative control, exhibited no inhibitory activity against either fungal strain, confirming that the solvent did not interfere with the bioassay. Among the synthesized derivatives, compound 7f emerged as the most potent against *C. albicans*, producing a zone of inhibition of 24 mm with an MIC of 3.12 µg/mL, closely approaching the activity of the standard drug Fluconazole (25 mm, MIC 2 µg/mL). Against *A. niger*, compounds 7d and 7f exhibited superior antifungal activity compared to Fluconazole. In particular, compound 7d showed the highest zone of inhibition (21 mm) and an MIC of 6.25 µg/mL, indicating excellent broad-spectrum antifungal efficacy. Compounds 7b and 7g also demonstrated good antifungal activity, whereas compound 7c was the least active derivative, exhibiting the smallest inhibition zones (12 mm against C. *albicans* and 10 mm against A. *niger*) and requiring a comparatively high MIC of 100 µg/mL against both fungal strains. Overall, the findings presented in (Table 5) suggest that the nature and position of the substituents significantly influence antifungal activity by affecting target interactions and cellular permeability, identifying compounds 7f and 7d as promising lead molecules for further structural optimization and biological investigation.

Table 5 Antifungal activity of the synthesized compounds (7a–g)

Compound Code	Zone of Inhibition (mm)C. albicans	Zone of Inhibition (mm)A. niger	MIC (µg/mL)C. albicans	MIC (µg/mL)A. niger
7a	16	13	25	50
7b	22	19	6.25	12.5
7c	12	10	100	100
7d	23	21	6.25	6.25

7e	15	12	50	50
7f	24	20	3.12	6.25
7g	21	18	12.5	12.5
Flucanazole	25	18	2	16
DMSO	0	0	–	–

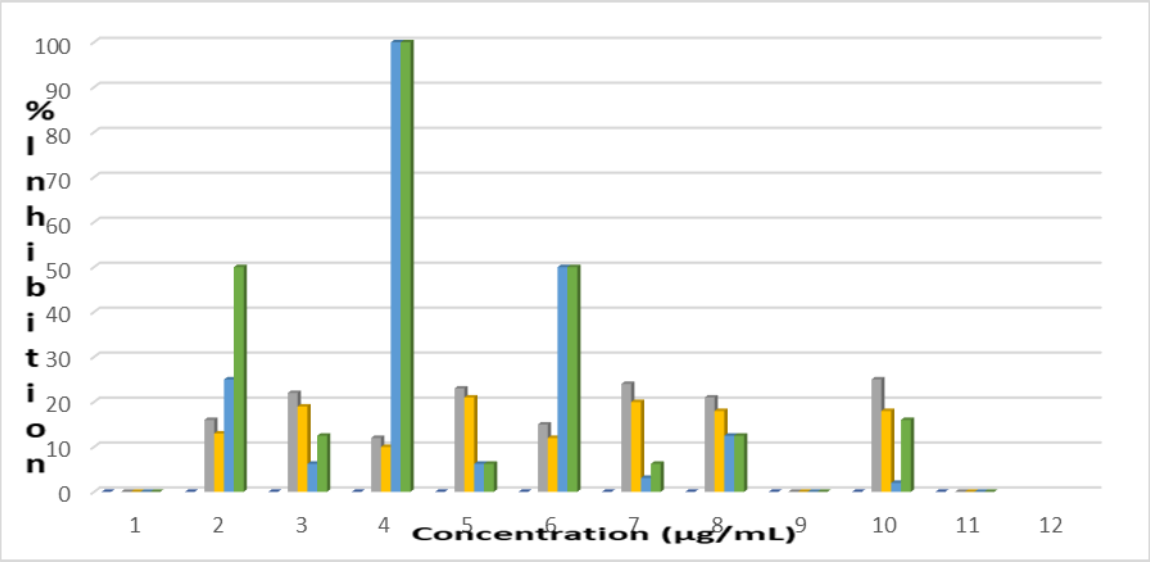


Fig 4. Graphical representation of % inhibition and concentration of the compounds (7a-g)

In Vitro Anti-inflammatory Activity

The in vitro anti-inflammatory activity of the synthesized pyrazoline derivatives (7a–7g) was evaluated using the albumin denaturation inhibition method, with diclofenac sodium serving as the reference drug. The percentage inhibition of protein denaturation was assessed at concentrations of 20, 40, 80, 200, and 400 µg/mL. The results demonstrated a concentration-dependent increase in the inhibition of albumin denaturation for all the tested compounds. Among the synthesized derivatives, compound 7f exhibited the highest percentage inhibition at all tested concentrations, with values ranging from 30.15 ± 0.29% at 20 µg/mL to 90.45 ± 0.38% at 400 µg/mL. Compounds 7a and 7e also demonstrated considerable anti-inflammatory activity, reaching 88.92 ± 0.40% and 87.60 ± 0.36% inhibition, respectively, at 400 µg/mL. Compound 7d showed moderate activity, followed by compounds 7g, 7b, and 7c. Compound 7c exhibited the lowest inhibitory activity among the synthesized derivatives at the tested concentrations.

Diclofenac sodium demonstrated the highest percentage inhibition at each concentration, increasing from 38.12 ± 0.25% at 20 µg/mL to 94.50 ± 0.38% at 400 µg/mL. These findings indicate that although the synthesized pyrazoline derivatives exhibited promising concentration-dependent anti-inflammatory activity, their inhibitory effects were generally lower than that of the reference drug.The IC_{50} values further supported the observed activity pattern. Among the synthesized compounds, 7f exhibited the lowest IC_{50} value (68.10 ± 0.36 µg/mL), followed by 7a (72.45 ± 0.38 µg/mL), 7e (76.18 ± 0.34 µg/mL), 7d (81.62 ± 0.31 µg/mL), 7g (83.40 ± 0.30 µg/mL), 7b (88.75 ± 0.32 µg/mL), and 7c (96.34 ± 0.35 µg/mL). Diclofenac sodium exhibited the lowest IC_{50} value of 38.25 ± 0.30 µg/mL, indicating greater potency than the synthesized derivatives under the experimental

conditions.Overall, compound 7f emerged as the most active derivative in the synthesized series, followed by 7a and 7e. The ability of these compounds to inhibit albumin denaturation suggests their potential as candidates for further anti-inflammatory investigation. However, additional studies involving appropriate cellular and in vivo models are required to establish their biological efficacy and mechanism of action.(Table 6)

Table :6 Anti inflammatory activity of the synthesized compounds (7a-7g)

Concentration (µg/mL)	7a	7b	7c	7d	7e	7f	7g	**Standard (Diclofenac Sodium)**
20	29.45±0.32	26.85±0.24	26.12±0.28	27.84±0.25	28.90±0.27	30.15±0.29	27.2±0.26	38.12±0.25
40	39.82±0.28	37.10±0.28	36.50 ±0.31	37.90±0.30	38.85±0.29	41.20±0.32	37.65±0.29	51.40±0.31
80	52.14±0.36	49.45±0.31	48.92±0.27	50.25±0.28	51.30±0.35	53.85±0.34	50.10±0.32	64.85±0.29
200	68.50±0.45	63.80±0.37	62.45±0.39	65.12±0.34	66.95±0.40	70.12±0.40	64.90±0.38	79.30±0.42
400	88.92±0.40	85.20±0.35	84.10±0.42	86.45±0.39	87.60±0.36	90.45±0.38	86.15±0.33	94.50±0.38
IC_{50}	72.45±0.38	88.75±0.32	96.34±0.35	81.62±0.31	76.18±0.34	68.10±0.36	83.40±0.30	38.25±0.30

Comparative studies of cathepsin K inhibitor, anti-inflammatory activity, anti-diabetic and anti -fungal

The biological evaluation of the synthesized phenacetamido- pyrazoline derivatives (7a–7g) revealed distinct structure-dependent activity profiles across cathepsin K docking, anti-inflammatory, antidiabetic and antifungal studies. In the context of osteoporosis, cathepsin K represents an important therapeutic target because of its role in osteoclastic degradation of the bone matrix, while inflammatory mediators such as TNF-α, IL-1β, and IL-6 can promote osteoclast differentiation and contribute to inflammation-associated bone loss. Among the synthesized derivatives, compound 7f exhibited the most favorable predicted binding energy against cathepsin K (−7.32 kcal/mol), suggesting that it warrants further investigation as a potential antiresorptive candidate. Its biological profile was further supported by the albumin-denaturation assay, in which 7f showed the lowest IC_{50} among the synthesized compounds (68.10 ± 0.36 µg/mL), followed by 7a (72.45 ± 0.38 µg/mL) and 7e (76.18 ± 0.34 µg/mL). Although these results indicate promising preliminary anti-inflammatory activity, diclofenac sodium remained more potent, with an IC_{50} of 38.25 ± 0.30 µg/mL. The COX-2 docking results also revealed favorable predicted binding for 7b (−9.74 kcal/mol), although 7f exhibited a more negative docking score (−9.93 kcal/mol), demonstrating that computational binding energies do not necessarily correspond directly to experimental anti-inflammatory potency. In the antidiabetic screening, compound 7c emerged as the most potent α-amylase inhibitor, with an IC_{50} of 25.60 ± 0.88 µg/mL, compared with 46.18 ± 0.75 µg/mL for the reference standard, whereas 7f showed an IC_{50} of 40.94 ± 0.92 µg/mL. The strong α-amylase inhibitory activity of 7c suggests potential for further investigation of carbohydrate-digestion inhibition, although its relevance to glycemic control requires additional validation. Notably, 7c exhibited comparatively weak anti-inflammatory and antifungal activities, indicating that the structural features favoring α-amylase inhibition may differ from those responsible for the other observed biological effects. In the antifungal assessment, compound 7f demonstrated the strongest activity against *Candida albicans*, with an inhibition zone of 24 mm and a minimum inhibitory concentration (MIC) of 3.12 µg/mL, approaching the activity of fluconazole. Against *Aspergillus niger*, compound 7d showed the largest inhibition zone (21 mm), while both 7d and 7f exhibited MIC values of 6.25 µg/mL, compared with 16 µg/mL for fluconazole under the reported experimental conditions. These findings suggest that 7f possesses a comparatively broad preliminary biological profile, whereas 7c and 7d display more pronounced activity in specific assays. From a structure–activity relationship perspective, the

differences among the derivatives may reflect variations in molecular interactions, physicochemical properties and target-specific recognition. The combination of favorable cathepsin K docking, anti-inflammatory screening activity and antifungal activity makes 7f a priority candidate for further investigation, particularly in studies exploring its potential effects on osteoclastic bone resorption and inflammation-associated skeletal damage. Nevertheless, the present findings do not establish direct cathepsin K inhibition, suppression of inflammatory cytokines or therapeutic efficacy against osteoporosis, diabetes, or fungal infections. Direct enzyme-inhibition studies, osteoclast-based bone-resorption assays, inflammatory mediator analysis, additional antidiabetic investigations and antifungal susceptibility testing are therefore necessary to confirm the biological relevance and therapeutic potential of the synthesized derivatives.

3.7 *In silico ADMET* study

ADME stands for absorption, distribution, metabolism and excretion. The body's ability to absorb, distribute, break down and remove a medication determines how effective it is. SwissADME is a reliable online tool that lets you calculate a substance's chemical similarity to a medication and its physiological effects. The ADME properties of ligands and complexes were examined in order to comprehend how structural modifications affect a complex's biological activity. Bioavailability radar (BR), which is widely used to quickly assess how similar something is to a medicine, looks at six physicochemical variables. Lipophilicity, size, polarity, solubility, flexibility and saturation are some of these variables.

Swiss ADME analysis indicates that's all the synthesized compounds (7a-7f) follow Lipinski's rule of five suggesting good oral drug-likeness their calculated log P values (4.34-5.97),molecular weights (504.49-520.36) ,hydrogen-bond donors (1) and hydrogen-bond acceptors(3,4,5) are within acceptable ranges. All the compounds show moderate predicted bioactivity with a bioavailability Radar (fig 4). Compound 7f , which exhibits the strongest binding to 1ATK in docking studies ,also diplays an ideal balance of liphophilicity, molecular size and polarity,emphasizing its potential as a lead compound. The combination of favourable ADME properties and high receptor affinity makes compound the most promising candidate for further development as an anti -diabetic, anti-fungal agent. Detailed ADMET data are provided in (Table 7).

Table 7 Complete ADMET profile of compounds (7a-g), including pharmacokinetics, physicochemical properties, lipophilicity, water solubility, drug-likeness and medicinal chemistry.

Ligand	Chemical Formula	Swiss ADME Filters							
		Molar mass (g/mol)	H bond acceptor	H bond donor	iLogP	Water Solubility mg/ml	GI absorption	TPSA (Å2)	Drug-likeness
7a	$C_{28}H_{21}BrClN_3O_2S$	518.91	3	1	4.34	7.47	High	90.01	No
7b	$C_{28}H_{21}Br_2N_3O_2S$	520.36	3	1	4.55	7.78	High	90.01	No
7c	$C_{30}H_{27}BrN_4O_2S$	513.35	3	1	4.42	7.12	High	93.25	No
7d	$C_{30}H_{27}BrClN_3O_2S$	509.98	3	1	5.91	7.45	High	90.01	No
7e	$C_{28}H_{21}BrFN_3O_2S$	512.45	4	1	5.97	7.03	High	90.01	No
7f	$C_{30}H_{26}BrN_3O_4S$	514.51	5	1	4.78	7.02	High	99.34	No
7g	$C_{29}H_{24}BrN_3O_3S$	504.49	4	1	4.36	6.95	High	99.24	No

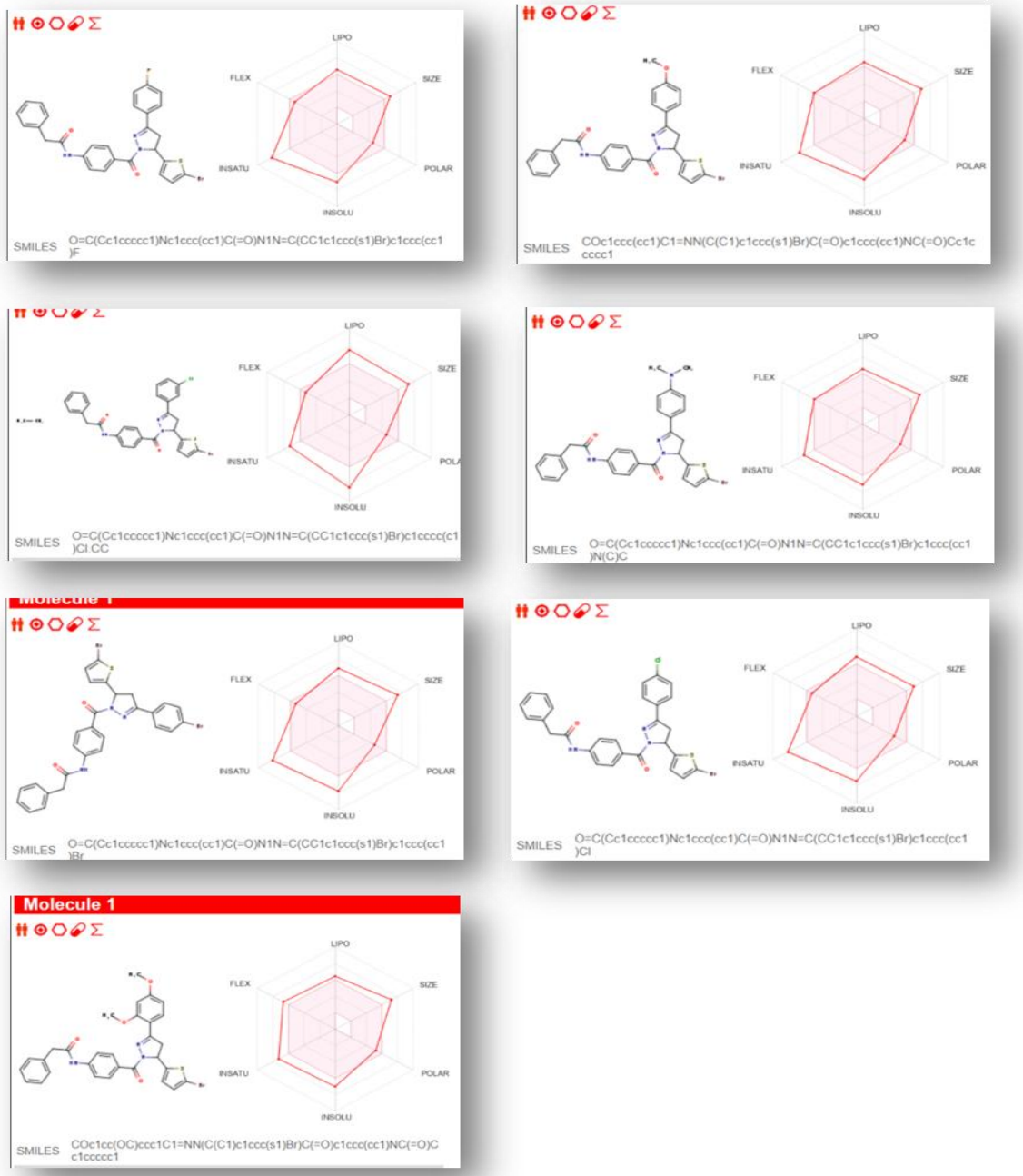


Fig 5. Bioavailability radar of the compounds (7a-g)

3.8. ProTox-III study

The toxicity profiles of the seven compounds were predicted using the ProTox-III online server. The predicted oral acute toxicity (LD_{50}) values ranged from 500 to 1000 mg/kg body weight, placing all compounds in toxicity class IV, indicating compounds that are harmful if swallowed but exhibit relatively low acute toxicity. Among the seven compounds, Compounds 7a, 7f and 7g were predicted to be inactive against all evaluated toxicity endpoints, including hepatotoxicity, cardiotoxicity, immunotoxicity, mutagenicity and cytotoxicity, suggesting a favorable safety profile. In contrast, Compounds 7b, 7c, 7d and 7e were predicted to exhibit hepatotoxicity with probability scores ranging from 0.52 to 0.56, while remaining inactive for cardiotoxicity and cytotoxicity. Compound 4 demonstrated the highest predicted toxicity, showing positive predictions for hepatotoxicity (0.56),

immunotoxicity (0.93) and mutagenicity (0.93). Similarly, Compound 5 was predicted to be hepatotoxic (0.56) and immunotoxic (0.81), although it was predicted to be non-mutagenic and non-cytotoxic.

Toxicity predictions further support the selection of Compound 7f. Although Compounds 7a and 7g showed favorable safety profiles, 7f demonstrated the best overall balance of docking affinity and predicted toxicity. In contrast, Compounds 7b–7e showed predicted hepatotoxicity (0.52–0.56), while Compounds 7d and 7e presented greater toxicological concerns, including immunotoxicity. Compound 7d also showed a high mutagenicity probability (0.93). Overall, Compound 7f emerged as the most promising candidate, combining strong binding to 1ATK with favorable predicted safety profiles. However, the moderate prediction accuracy (54.26%) and similarity values (45.54–49.10%) indicate that these computational results are preliminary and require experimental validation (Table 8).

Table 8 Protox -III Toxicological profiles oral organ and end toxicity

Compound No	Const.LD50 dose (mg/kg)	Prediction toxicity						Average similarity	Prediction Accuracy
		The toxicity prediction criteria and % probability value of bioactive molecules							
	prediction	class	Hepato	Cardio	Immuno.	Mutag.	Cyto.	%	%
7a	1000	4	Inactive (0.5)	Inactive (0.74)	Inactive (0.99)	Inactive (0.65)	Inactive (0.65)	49.1	54.26
7b	1000	4	Active (0.52)	Inactive (0.74)	Inactive (0.99)	Inactive (0.65)	Inactive (0.65)	45.8	54.26
7c	500	4	Active (0.54)	Inactive (0.69)	Inactive (0.99)	Inactive (0.65)	Inactive (0.65)	46.05	54.26
7d	1000	4	Active (0.56)	Inactive (0.70)	Inactive (0.99)	Active (0.93)	Inactive (0.56)	46.37	54.26
7e	1000	4	Active (0.56)	Inactive (0.73)	Active (0.81)	Inactive (0.62)	Inactive (0.59)	47.56	54.26
7f	500	4	Inactive (0.50)	Inactive(0.74)	Inactive(0.99)	Inactive(0.65)	Inactive(0.68)	45.54	54.26

7g	500	4	Inactive(0.50)	Inactive(0.74)	Inactive(0.99)	Inactive (0.65)	Inactive(0.68)	46.37	54.26

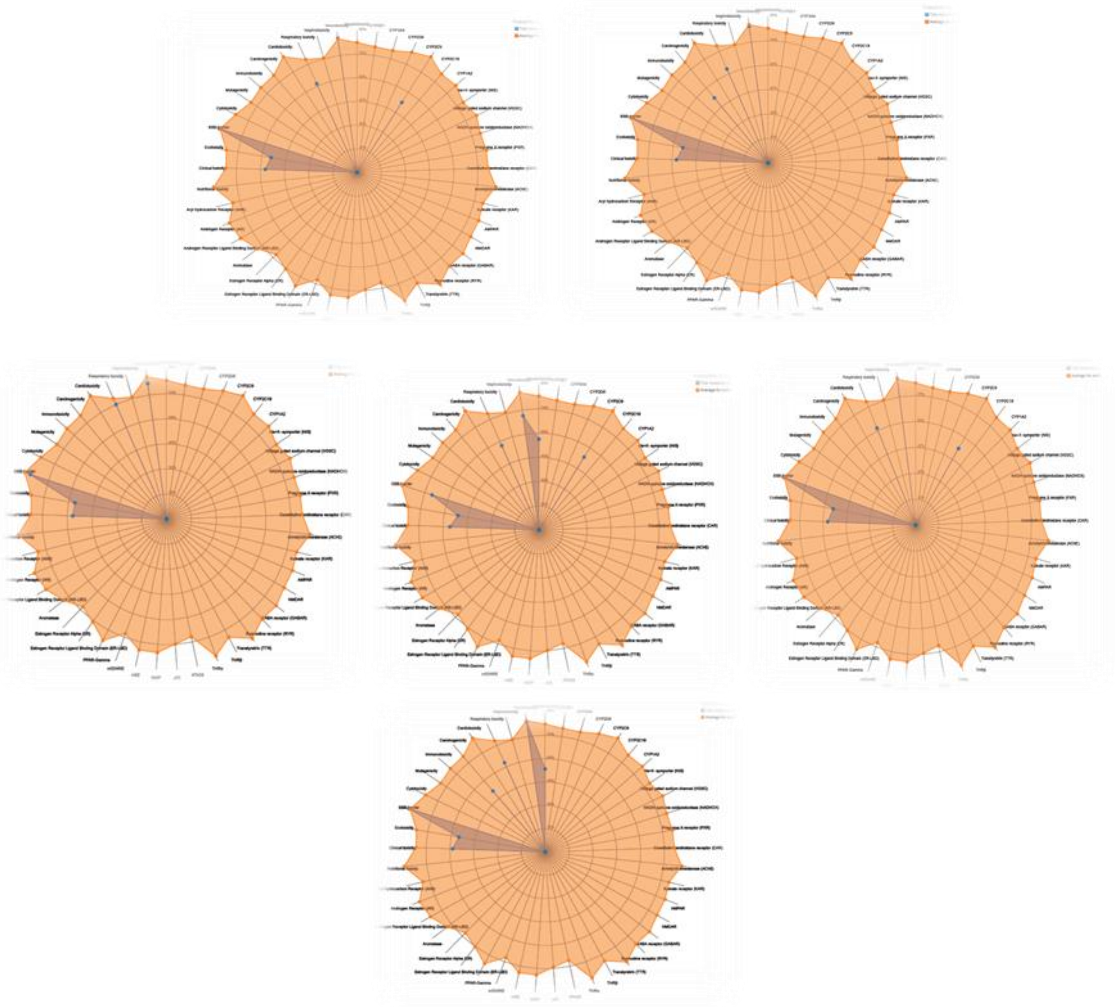


Fig 6. Overall toxicity radar chart of compound (7a-g)

3.9. Frontier molecular orbital analysis and correlation with biological activity

Frontier molecular orbital (FMO) theory was used to describe the electrical parameters governing the biological behavior and reactivity of the generated compounds (7a-7g). The highest occupied molecular orbital of a molecule represents its capacity to contribute electrons. (HOMO), whereas it's lowest unoccupied molecular orbital (LUMO) represents its ability to accept electrons. The HOMO–LUMO energy gap (ΔE) is an important measure of molecular reactivity; larger gaps indicate greater electronic stability, whereas smaller gaps are generally associated with better polarizability and chemical reactivity. (Table 9) summarizes the computed HOMO, LUMO and ΔE values. The ΔE values show moderate electrical flexibility across the sequence, ranging from 0.029 to 0.07016 eV. Compound 7a has the smallest energy gap (ΔE = 0.029 eV), indicating lower thermodynamic stability and greater inherent chemical reactivity. Nevertheless, compound 7a showed only moderate docking scores and in vitro anti-diabetic and anti-fungal actions despite its increased electronic reactivity, suggesting that high electronic softness by itself does not always result in better biological binding.

Compound	HOMO	LUMO	ΔE

7a	-0.11393	-0.08442	0.029
7b	-0.13801	-0.07988	0.0581
7c	-0.19595	-0.16355	0.0323
7d	-0.19648	-0.16398	0.0325
7e	-0.19572	-0.16302	0.0327
7f	-0.21744	-0.14728	0.0701
7g	-0.18768	-0.15469	0.03295

Table 9 Frontier Molecular Orbital values of the compound (7a-g)

Compound 7f, on the other hand, has a somewhat higher ΔE value (0.07016 eV) and the strongest binding affinity toward the cathepsin inhibitor as well as the highest in vitro anti inflammatory, anti-diabetic and anti-fungal effects. An ideal balance between electronic stability and reactivity is reflected in this moderate HOMO–LUMO gap, which is advantageous for long-term and targeted receptor–ligand interactions. Compounds 7g and 7b exhibited matching intermediate docking affinities and biological responses, with intermediate ΔE values of (0.058136 and 0.3299 eV), respectively.

These findings imply that successful biological activity requires an ideal range of ΔE rather than the smallest gap. Reduced ΔE increases molecular reactivity, but too small energy gaps might cause nonspecific interactions or jeopardize structural stability. On the other hand, selective binding and better pharmacological activity seem to be favored by a somewhat greater ΔE.This association is further supported by the geographical distribution of the HOMO and LUMO orbitals. Compound 7f displays a more regulated orbital distribution that promotes stable receptor engagement, while compound 7a displays substantial orbital delocalization, which is consistent with its high reactivity, as shown in (Fig. 6). Overall, the FMO analysis supports the docking and biological data by showing that electronic structure is essential for controlling the cathepsin inhibitor under the synthetic phenacetamido-pyrazoline derivatives anti-diabetic and anti-fungal properties.

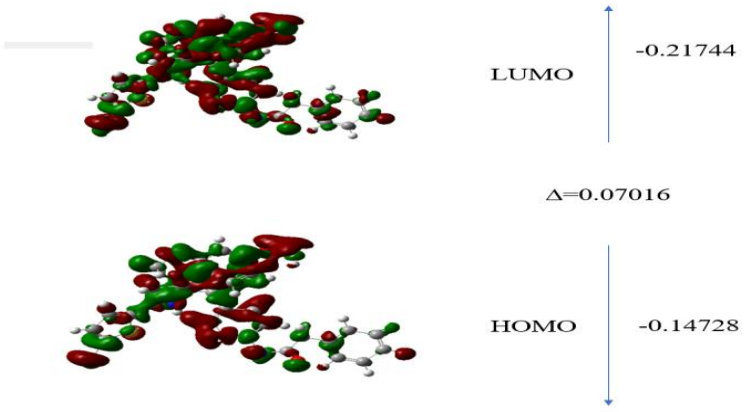


Fig 7: HOMO-LUMO images of the compound 7f

4. Conclusion

An ionic liquid-supported workup is used to synthesise a novel series of phenacetamido-pyrazoline derivatives, offering a sustainable and eco-friendly substitute for traditional techniques. According to molecular docking studies and in vitro anti-diabetic and anti-fungal tests, compound 7f was found to have the strongest anti-diabetic and anti-fungal activity, anti-inflammatory activity, among the compounds (1ATK and COX-2). Their drug-like potential is supported by *insilico ADMET* and Protox-III analyzes, which show favorable pharmacokinetic profiles and minimal projected toxicity. Electronic characteristics that are correlated with biological activity and reactivity are revealed by DFT calculations and frontier molecular orbital (FMO)

research. Overall, these findings show that phenacetamido-pyrazoline derivatives have therapeutic potential and emphasize the importance of ionic liquid-mediated green synthesis in drug discovery. Compound 7f stands out as a promising candidate for additional preclinical testing to investigate its pharmacological potential.

5. Experimental

5.1 General

All chemicals and solvents were purchased from Sigma-Aldrich, Avra and TCI Chemicals were used as received without further purification. Melting points were determined using open-capillary tubes. The purity of the compounds and the progress of the reactions were monitored by thin-layer chromatography (TLC) on silica gel plates under UV light. The mobile phase consisted of a petroleum ether and ethyl acetate solvent system in a 1:3 ratio. Infrared (IR) spectra were recorded in the range of 4000–600 cm^{-1} using an Agilent Resolution spectrometer. ^{1}H and ^{13}C NMR spectra were recorded on a Bruker 400 MHz NMR spectrometer at room temperature using $CDCl_3$ or DMSO-d_6 as solvents. Tetramethylsilane (TMS) was used as the internal standard and chemical shifts were reported in parts per million (ppm).

5.2 Synthesis

5.2.1 General procedure for the synthesis of chalcone (3a-g)

The condensation reaction between 2 Acetyl -5-bromothiophene (1.0 mmol) and various substituted benzaldehydes (1.5 mmol) in stoppered conical flask. An equimolar mixture of the reactants is dissolved in 80 ml ethanol. To facilitate the reaction, Sodium hydroxide NaOH) was added. The reaction mixture was then stirred for 6-8 hours. The progress of the reaction is diligently monitored using Thin-Layer Chromatography (TLC), employing a solvent system of ethyl acetate and petroleum ether in a 1:3 ratio. Upon completion of the reaction, as indicated by TLC, the mixture is carefully poured into crushed ice. This step aided in the precipitation of the crude Chalcone. The precipitate is then filtered and recrystallized using methanol to obtain the purified chalcone products.

5.2.2 General procedure for the synthesis of pyrazoline (5a-g)

In a round-bottom flask equipped with a magnetic stir bar and a reflux condenser, the chalcone derivative [3a–g] (1.0 mmol) and 4-aminobenzohydrazide 4 (1.1mmol) are dissolved in methanol (15-20 mL), followed by the addition of potassium hydroxide (KOH, (1.2mmol). The reaction mixture is heated under reflux with continuous stirring and monitored by Thin-Layer Chromatography (TLC) until completion (4-8hrs). Once completed, the mixture is cooled to room temperature, poured into ice-cold water under vigorous stirring to precipitate the product, and the resulting solid 5a–g is isolated via vacuum filtration, washed thoroughly with cold water, dried, and recrystallized from hot ethanol.

5.2.3 General procedure for the synthesis of phenacetamido – pyrazoline (7a-g)

The appropriate pyrazoline intermediate 5a–g (1.0 mmol) was dissolved in dichloromethane (DCM, 10 mL) in a reaction flask containing the ionic liquid 1-allyl-3-methylimidazolium bromide [AMIM](Br), (1.0 mmol). The mixture was cooled in an ice bath before phenylacetyl chloride (1.1 mmol) was added dropwise. The reaction mixture was then warmed to room temperature and stirred continuously for 2–5 hours, with the progress of the reaction monitored by thin-layer chromatography (TLC). Upon completion, the mixture was diluted with additional DCM and washed sequentially with water and saturated sodium bicarbonate ($NaHCO_3$) solution. The organic layer was separated, dried over anhydrous sodium sulfate (Na_2SO_4), filtered and concentrated under reduced pressure. The resulting crude product was purified by recrystallization from ethanol to afford the pure target compounds (7a–g). After the extraction process, the immiscible ionic liquid catalyst was separated from the reaction medium, washed thoroughly with diethyl ether, dried under vacuum and preserved for subsequent recycling runs.

Spectral data for the compounds.

1-(4-(2-phenylacetamido)benzoyl)-3-(5-bromothiophen-2-yl)-5-(4-chlorophenyl)pyrazoline

Brown solid ;Molecular formula :$C_{28}H_{21}BrClN_3O_2S$,IR(KBr cm^{-1}) (1662)(C=Oin phenacetamide), N-H(3250 phenacteamide),(1600)(C=N in pyrazoline),1535(C=C),^{1}HNMR (400 MHz, DMSO-d6) (ppm): 10.55(NH),7.92–7.15(Ar-H),(PyrazolineC5-H),3.84(Pyrazoline CH), 3.65(CH_2CO). 13CNMR, 48.88 (C_4, pyrazoline), 52.33 (C_5,pyrazoline), 112.75 (CBr), 118.9-144.07 (aromaticcarbons), 136.09(ipsocarbon), 166.27(C=N), 169.70 (C=O) (phenacetamide),170.21(C=O).

1-(4-(2-phenylacetamido)benzoyl)-3-(5-bromothiophen-2-yl)-5-(4-bromophenyl)pyrazoline

Yellow solid: Molecular formula$C_{28}H_{21}Br_2N_3O_2S$: IR (KBr, vmax, cm^{-1}) 3250 (N–H phenacetamide), 1650 (C=O phenacetamide), 1595 (C=N pyrazoline), 1520 (C=C). ^{1}H NMR (400 MHz, DMSO-d6) δ10.54 (NH-), 7.89–7.19 (Ar-H), 5.75 (pyrazoline-C5-H), 3.70 (pyrazoline-C4), 3.65 (CH_2-Ph).^{13}CNMR (DMSO):173.22 (C=O,amide), 135.63-118.23 (AromaticCarbons), 142.50 (PyrazolineC=N), 45.93 (Pyrazoline CH_2)41.31 (pyrazolineCH), (CH_2CO)(43.80).

1-(4-(2-phenylacetamido)benzoyl)-3-(5-bromothiophen-2-yl)-5-(4-(dimethylamino)phenyl)pyrazoline

Orange solid: Molecular formula: $C_{22}H_{21}BrN_4OS$, IR(KBr cm^{-1}):3250(N-Hphenacetamide),1662(C=O phenacetamide),C=N(1595 pyrazoline), 1490 (C=C),^{1}H NMR :2.96(CH_2), 3.85(CH)6.61-7.95 (Ar-H), N(CH_3)$_2$(3.08) N-H (9.73). 13C NMR: 40.87 [N(CH_3)$_2$], 45.39 (C_4, pyrazoline), 52.01 (C_5, pyrazoline), 112.75 (C–Br), 111.02-142.15 (aromatic carbons), 141.77, 143.92 (ipso carbons), 154.40 (C=N), 169.55(C=O) (phenacetamide).

1-(4-(2-phenylacetamido)benzoyl)-3-(5-bromothiophen-2-yl)-5-(2-chlorophenyl)pyrazoline

Brown solid; Molecular formula :$C_{28}H_{21}BrClN_3O_2S$,IR(KBr cm^{-1}) (C=O)(1654 phenacetamide)(,N-H(3287 phenacetamide),(C=N)(1600 pyrazoline),(1520)(C=C),^{1}HNMR (400 MHz, DMSO-d_6) (ppm): 10.55 (NH), 7.92–7.74 (Ar-H), 5.60(PyrazolineC5-H), 3.84 (Pyrazoline CH), 3.65(CH_2CO). 13CNMR (400MHz, DMSOd_6) (ppm):48.88 (C_4,pyrazoline), 52.33(C_5,pyrazoline), 112.75(CBr), 118.96-144.07 (aromaticcarbons), 166.27 (C=N),169.70(C=O)(phenacetamide).

1-(4-(2-phenylacetamido)benzoyl)-3-(5-bromothiophen-2-yl)-5-(4-fluorophenyl)pyrazoline

Reddish brown solid: Molecular formula: $C_{28}H_{21}BrFN_3O_2S$: IR (KBr, vmax, cm^{-1}): 3220 (N–H phenacetamide), 1640 (C=O phenacetamide), 1580 (C=N pyrazoline), 1502 (C=C). ^{1}H NMR (400 MHz, DMSO-d_6) ; 10.44 (NH), 7.93 -7.16(Ar-H) 5.54 (CH-pyrazoline), 3.96 (CH_2-pyrazoline), 3.68 ($COCH_2$,): ^{13}C NMR 169.5 (C=O, amide), 164.2 (C=O, pyrazoline carbonyl), 149.8 (C=N), 142.8-118.2(Aromatic carbons), 59.4 (CH-pyrazoline), 43.6 ($COCH_2$), 42.5 (CH_2-pyrazoline).

1-(4-(2-phenylacetamido)benzoyl)-3-(5-bromothiophen-2-yl)-5-(2,4-dimethoxyphenyl)pyrazoline

Yellowish solid: Molecular formula: $C_{30}H_{26}BrN_3O_4S$: IR (KBr, vmax, cm^{-1}): 3287 (N–H phenacetamide), 1654 (C=O phenacetamide), 1600 (C=N pyrazoline), 1525 (C=C). ^{1} H NMR (400 MHz, DMSO-d_6) : 10.52 (NH), 7.91 -6.53(Ar-H), 5.58 (Pyrazoline-C5-H), 3.87, 3.84 (-OCH_3), 3.65 (-CH_2-Ph), 3.56 (Pyrazoline-C4-H) .^{13}C NMR (100 MHz, DMSO d_6) : 173.2 (C=O), 135.53 (C=N) 135.1 (Ar-C), 130.13- 118.80 (Ar-CH), 52.5 (CH) 45.96 (CH_2), 42.20(CH_2CO).

1-(4-(2-phenylacetamido)benzoyl)-3-(5-bromothiophen-2-yl)-5-(4methoxyphenyl)pyrazoline derivative

Brown solid; Molecular formula:$C_{29}H_{24}BrN_3O_3S$: IR (KBr, vmax, cm^{-1}): 3272 (N–H in phenacetamide), 1670 (C=O in phenacteamide), 1602 (C=N pyrazoline), 1520 (C=C) :^{1}H-NMR (400 MHz, DMSO-d6) : 10.50 (N-H), 7.67 – 6.91 (Ar-H), 3.98 (PyrazolineCH_2), 3.60 (Pyrazoline CH), 3.47(CH_2CO) ^{13}C NMR (DMSO-d6): 173.3, 170.3(C=O) 166.3 (pyrazoline C=N), 144.2- 114.5 (Aromatic carbons), 55.6 (OCH3), 52.5 (Pyrazoline CH), 43.8 (CH-Ph), 42.2 (Pyrazoline CH_2).\

5.3 Biology

5.3.1 Anti-diabetic

α-amylase inhibition technique.

The samples anti-diabetic activity was assessed utilising the inhibition of α-amylase technique. In a nutshell, amylase (0.2%) was incubated for 10 min at 25 ºC with and without samples (in 1.5 mL) and the standard. This test was conducted in a phosphate buffer of 0.2 M. (pH 6.9). The 1% starch solution (0.5 mL) was added after the pre-incubation period, and the reaction mixture was then incubated for 30 min at 25ºC. The DNSA reagent (0.5 mL) was added as the colour reagent to stop the enzymatic reaction, and the mixture was then incubated in a boiling water bath for 90 min. A UV–Visible spectrophotometer was used to measure the absorbance at 540 nm after the samples were diluted in 2.5 mL of distilled water and allowed to cool to room temperature. The measured absorbance was compared with that of the control experiment. The percentage inhibition was calculated from the given formula [27,33,30].

$$\%\ of\ Inhibition = 100 \times [Ac\ .\ At\ /Ac]$$

At: Absorbance of test.

Ac: Absorbance of control.

5.3.2 Anti-fungal activity

The preliminary in vitro antifungal was evaluated using the agar well diffusion [or disc diffusion] method against standard pathogenic strains. Sabouraud Dextrose Agar (SDA) plates were prepared and uniformly inoculated by continuous swabbing with a fungal suspension containing approximately 1×10^6 CFU/mL of the respective organism.The test compounds were dissolved in 100% analytical grade DMSO to yield a stock concentration of 1 mg/mL. For the well diffusion assay, wells of 6 mm diameter were bored into the agar medium using a sterile cork borer, and 50 µg L of the compound solution was loaded into each well. [Alternatively, for disc diffusion: Sterile Whatmann No. 1 filter paper discs (6 mm diameter) were impregnated with 20 µg L of the compound solution, allowed to dry under aseptic conditions and placed onto the inoculated agar surface.] Pure DMSO was used as the negative solvent control, while Fluconazole (10 µg/disc) was used as the positive reference drug. The plates were incubated at 28 °C [or 35 °C] for 48 h. The antifungal efficacy was quantified by measuring the diameter of the zone of inhibition (ZOI) in millimeters (mm) using a digital caliper. All experiments were performed in triplicate, and the results were expressed as mean SD [33].

5.3.3. Anti-inflammatory activity

BSA Techniques

The prepared pyrazoline compounds and the reference drug diclofenac sodium were assessed for their anti-inflammatory activity using a modified albumin denaturation inhibition method with minor adjustments (28,29). The reference drug and the synthesized pyrazoline derivatives were first solubilized in a small volume of dimethylformamide (DMF), followed by dilution using phosphate buffer solution (0.2 M, pH 7.4).

The final concentration of DMF in all prepared solutions was maintained below 2.5% .A 2.5 mL test solution containing various concentrations of the pyrazoline compounds was mixed with 1 mL of 1 mM bovine serum albumin (BSA) solution prepared in phosphate bufferThe reaction mixtures were incubated at 37 °C for 10 minutes. Protein denaturation was subsequently induced by heating the mixtures at 70 °C for 10 minutes in a water bath. After cooling the samples to room temperature, turbidity was measured spectrophotometrically at 660 nm. The percentage inhibition of albumin denaturation was calculated by comparing the absorbance of the test samples with that of the control, which contained no drug.

$$\%\ of\ Inhibition = 100\ x\ [\ Ac\text{-}At\ /Ac]$$

At: Absorbance of test

Ac: Absorbance of control

5.4 Molecular docking

The docking investigations were carried out to gain a better knowledge of the binding mechanisms of the synthesised derivatives (7a-g). The Protein Data Bank provided the 3D structures of the target proteins.PDB code: 1ATK and COX-2 (1CVU); Utilizing an empirical scoring function based on binding free energy, AutoDock 4.2 was used for the molecular docking research. Numerous stochastic search methods are offered by AutoDock. Utilizing the Lamarckian Genetic Algorithm was our initial choice (LGA). It combines both local and global search the 2D image captured by the BIOVIA Discovery Studio and the 3D image obtained [30-32]

5.5 *ADMET* studies

The Swiss ADME, which predicts physically and pharmaceutically significant aspects of organic molecules, was used to compute the Absorption, Distribution, Metabolism and Excretion, (ADME) characteristics of the drugs [31-33].

5.6 ProTox-III

The ProTox-III web server is a tool that predicts the potential toxicity of chemical compounds. It classifies toxicity into various types, including oral and liver toxicity (hepatotoxicity). It also predicts other harmful effects like mutagenesis, carcinogenicity, cytotoxicity and immunotoxicity (e.g., B cell inhibition). The server helps researchers understand how and why a compound might be toxic by identifying its potential toxic pathways (Adverse Outcome Pathways, or AOPs) and molecular targets [34].

Acknowlegements

The authors are thankful to Dr. R. Sribalan, Biochemie Innovations Lab for his helpful discussions in Anti-Diabetic, Anti-fungal.

Refrences

[1] Chemat, F., Abert Vian, M., Ravi, H. K., Khadhraoui, B., Hilali, S., Perino, S., & Fabiano Tixier, A. S. (2019). Review of alternative solvents for green extraction of food and natural products: Panorama, principles, applications and prospects. *Molecules*, *24*(16), 3007.

[2] Barasarathi, J., EA Zaki, M., Venkatesan, K., Karthikeyan, P., Wong, L. S., & Gomha, S. M. (2026). Recent progress in ionic liquid-catalyzed multicomponent reactions: a green and sustainable approach to organic synthesis in line with the UN SDGs. *Green Chemistry Letters and Reviews*, *19*(1), 2624188.

[3] Zhang, Q., Hu, Y., Li, S., Zhang, M., Wang, Y., Wang, Z., ... & Pan, H. (2022). Recent advances in supported acid/base ionic liquids as catalysts for biodiesel production. *Frontiers in Chemistry*, *10*, 999607.

[4] Wolny, A., & Chrobok, A. (2022). Silica-based supported ionic liquid-like phases as heterogeneous catalysts. *Molecules*, *27*(18), 5900.

[5] Tomar, P., & Jain, D. (2022). A review of green solvent IONIC liquids: as a future solvent. *Journal of Advanced Scientific Research*, *13*(06), 1-16.

[6] Rosenstock, J., Aggarwal, N., Polidori, D., Zhao, Y., Arbit, D., Usiskin, K., & Canagliflozin DIA 2001 Study Group. (2012). Dose-ranging effects of canagliflozin, a sodium-glucose cotransporter 2 inhibitor, as add-on to metformin in subjects with type 2 diabetes. *Diabetes care*, *35*(6), 1232-1238.

[7] Rodrigues, C. F., Rodrigues, M. E., & Henriques, M. (2019). Candida sp. infections in patients with diabetes mellitus. *Journal of clinical medicine*, *8*(1), 76.

[8] Kalinovskii, A. P., Sintsova, O. V., Gladkikh, I. N., & Leychenko, E. V. (2023). Natural inhibitors of mammalian α-amylases as promising drugs for the treatment of metabolic diseases. *International journal of molecular sciences*, *24*(22), 16514.

[9] Di Stefano, E., Oliviero, T., & Udenigwe, C. C. (2018). Functional significance and structure–activity relationship of food-derived α-glucosidase inhibitors. *Current Opinion in Food Science*, *20*, 7-12.

[10] Van de Laar, F. A., Lucassen, P. L., Akkermans, R. P., Van de Lisdonk, E. H., Rutten, G. E., & Van Weel, C. (2005). α-Glucosidase inhibitors for patients with type 2 diabetes: results from a Cochrane systematic review and meta-analysis. *Diabetes care*, *28*(1), 154-163.

[11] Abchir, O., Rossafi, B., Bouribab, A., Es-Sounni, B., Touti, R., Yamari, I., & Chtita, S. (2026). In Silico Design of Pyrimidine Derivatives as Potential α-Glucosidase Inhibitors: QSAR, Molecular Docking, ADMET, and Molecular Dynamics Studies. *International Journal of Molecular Sciences*, *27*(13), 5696.

[12] Vaez, A., Ghahremanzadeh, A., Zare, F., Nami, S., Zargari, F., Najafi, S., & Morovati, H. (2026). Global prevalence, mortality, and comorbidities of patients with diabetes mellitus and proven Candida auris emerging infection: a systematic review & meta-analysis. *BMC Infectious Diseases*, *26*(1), 535.

[13] Gupta, O., Pradhan, T., & Chawla, G. (2025). Structural and functional insights into PPAR-γ: Review of its potential and drug design innovations for the development of antidiabetic agents. *European Journal of Medicinal Chemistry*, 118264.

[14] Giannella, M., Lanternier, F., Dellière, S., Groll, A. H., Mueller, N. J., Alastruey-Izquierdo, A., & Slavin, M. A. (2025). Invasive fungal disease in the immunocompromised host: changing epidemiology, new antifungal therapies, and management challenges. *Clinical Microbiology and Infection*, *31*(1), 29-36.

[15] Zhang, M., Yang, W., Liu, N., Tu, J., Lin, J., Dong, G., & Sheng, C. (2025). Lanosterol 14α-demethylase (CYP51)/heat shock protein 90 (Hsp90) dual inhibitors for the treatment of invasive candidiasis. *Journal of Medicinal Chemistry*, *68*(2), 1668-1681.

[16] Saleem, A.; Khattak, S. U.; Ahmad, S.; Ahmad, A.; Alsagri, H. S.; Menshawi, A. Purification and Characterization of a Dihydroxy Oxocyclohexyl Acetate Derivative from Endophytic *Aspergillus candidus* Targeting *Candida albicans* Lanosterol 14α-Demethylase. *Sci. Rep.* **2026**, *16* (1), 5379.

[17] Osman, H., Arshad, A., Lam, C. K., & Bagley, M. C. (2012). Microwave-assisted synthesis and antioxidant properties of hydrazinyl thiazolyl coumarin derivatives. *Chemistry Central Journal*, *6*(1), 32.

[18] El-Sabbagh, O. I., Baraka, M. M., Ibrahim, S. M., Pannecouque, C., Andrei, G., Snoeck, R., & Rashad, A. (2009). Synthesis and antiviral activity of new pyrazole and thiazole derivatives. *European journal of medicinal chemistry*, *44*(9), 3746-3753.

[19] Kursun Aktar, B. S., Sıcak, Y., Bakırdöven, A., Tatar Yılmaz, G., Kaya, S., Karakucuk-Iyidogan, A., & Oruc-Emre, E. E. (2025). Novel Pyrrolidine-Based Pyrazolines as α-Glucosidase Inhibitors: Microwave-Assisted Synthesis, Antidiabetic Activity, In Silico ADMET Prediction, Molecular Docking, and Molecular Dynamics Simulations. *ACS omega*, *10*(39), 45450-45464.

[20] Menezes, R. A., & Bhat, K. S. (2025). Synthetic aspects, structural insights and pharmacological potential of pyrazole derivatives: an overview. *Discover Applied Sciences*, *7*(2), 137.

[21] Ibrahim, S. R., Omar, A. M., Bagalagel, A. A., Diri, R. M., Noor, A. O., Almasri, D. M., & Mohamed, G. A. (2022). Thiophenes—naturally occurring plant metabolites: Biological activities and in silico evaluation of their potential as cathepsin D inhibitors. *Plants*, *11*(4), 539.

[22] Matiadis, D., & Sagnou, M. (2020). Pyrazoline hybrids as promising anticancer agents: An up-to-date overview. *International Journal of Molecular Sciences*, *21*(15), 5507..

[23] Kursun Aktar, B. S., Sıcak, Y., Bakırdöven, A., Tatar Yılmaz, G., Kaya, S., Karakucuk-Iyidogan, A., & Oruc-Emre, E. E. (2025). Novel Pyrrolidine-Based Pyrazolines as α-Glucosidase Inhibitors: Microwave-Assisted Synthesis, Antidiabetic Activity, In Silico ADMET Prediction, Molecular Docking, and Molecular Dynamics Simulations. *ACS omega*, *10*(39), 45450-45464.

[24] Kumari, P., Mishra, V. S., Narayana, C., Khanna, A., Chakrabarty, A., & Sagar, R. (2020). Design and efficient synthesis of pyrazoline and isoxazole bridged indole C-glycoside hybrids as potential anticancer agents. *Scientific reports*, *10*(1), 6660.

[25] Moreno, L. M., Quiroga, J., Abonia, R., Ramírez-Prada, J., & Insuasty, B. (2018). Synthesis of new 1, 3, 5-triazine-based 2-pyrazolines as potential anticancer agents. *Molecules*, *23*(8), 1956.

[26] Verma, G., Marella, A., Shaquiquzzaman, M., Akhtar, M., Ali, M. R., & Alam, M. M. (2014). A review exploring biological activities of hydrazones. *Journal of pharmacy & bioallied sciences*, *6*(2), 69.

[27] Sribalan, R., Banuppriya, G., Kirubavathi, M., Jayachitra, A., & Padmini, V. (2016). Multiple biological activities and molecular docking studies of newly synthesized 3-(pyridin-4-yl)-1H-pyrazole-5-carboxamide chalcone hybrids. *Bioorganic & medicinal chemistry letters*, *26*(23), 5624-5630.

[28] Bhattacharjee, B., & Chatterjee, J. (2013). Identification of proapoptopic, anti-inflammatory, anti-proliferative, anti-invasive and anti-angiogenic targets of essential oils in cardamom by dual reverse virtual screening and binding pose analysis. *Asian Pac J Cancer Prev*, *14*(6), 3735-42.

[29] Adib, M., Peytam, F., Rahmanian-Jazi, M., Mohammadi-Khanaposhtani, M., Mahernia, S., Bijanzadeh, H. R., & Larijani, B. (2018). Design, synthesis and in vitro α-glucosidase inhibition of novel coumarin-pyridines as potent antidiabetic agents. *New Journal of Chemistry*, *42*(21), 17268-17278.

[30] Mahanthesh, M. T.; Ranjith, D.; Yaligar, R.; Jyothi, R.; Narappa, G.; Ravi, M. Swiss ADME Prediction of Phytochemicals Present in *Butea monosperma* (Lam.) Taub. *J. Pharmacogn. Phytochem.* **2020**, *9* (3), 1799–1809.

[31] Ramkumar, S., & Ramarajan, R. (2023). Design, synthesis, spectral characterization, multiple-biological activities, docking and in silico ADMET studies of thiazolidinones. *Results in Chemistry*, *5*, 100861.

[32] Merimi, C., Benabbou, A., Fraj, E., Khibech, O., Yahyaoui, M. I., Asehraou, A., & Almutairi, S. M. (2025). Valorization of imidazolium-based salts as next-generation antimicrobials: integrated biological evaluation, ADMET, molecular docking, and dynamics studies. *ASEAN Journal of Science and Engineering*, *6*(1), 11-34.

[33] Sharma, N.; Gupta, N.; Orfali, R.; Kumar, V.; Patel, C. N.; Peng, J.; Perveen, S. Evaluation of the Antifungal, Antioxidant, and Anti-Diabetic Potential of the Essential Oil of *Curcuma longa* Leaves from the North-Western Himalayas by In Vitro and In Silico Analysis. *Molecules* **2022**, *27* (22), 7664.

[34] Ezhilarasan, K.; Nagaraj, S.; Ramarajan, R. Ionic Liquid-Assisted Green Synthesis of Thiazole Derivatives with Enhanced Anti-Inflammatory Activity. *J. Mol. Liq.* **2026**, *418*, 129432.